Following the trail of new physics via the vector boson fusion Higgs boson signal at the Large Hadron Collider

Tisa Biswas,[1,*] Anindya Datta,[1,†] and Biswarup Mukhopadhyaya[2,‡]

[1]*Department of Physics, University of Calcutta, 92 Acharya Prafulla Chandra Road, Kolkata 700009, India*

[2]*Department of Physical Sciences, Indian Institute of Science Education and Research, Mohanpur 741246, India*

(Received 20 July 2021; accepted 28 February 2022; published 29 March 2022)

We investigate the modification of the Higgs signals from vector boson fusion at the LHC arising from higher-dimensional effective operators involving quarks, electroweak gauge bosons, and the 125 GeV scalar discovered in 2012. Taking a few of the admissible dimension-6 operators as illustration, we work within the framework of the Standard Model effective field theory (SMEFT) and identify kinematic variables that can reflect the presence of such effective operators. The useful variables turn out to be the geometric mean of the transverse momenta of the two forward jets produced in vector boson fusion and the rapidity difference between the two forward jets. We identify the shift in event population caused by the effective operators in the same, spanned by the above kinematic variables. Minimum values of the Wilson coefficients of the chosen dimension-6 operators are identified, for which they can be probed at the 3σ level in the high-luminosity run of the LHC at 14 TeV. Projected exclusion limits on some of the couplings, obtained from our analysis, can significantly improve the limits on such couplings derived from electroweak precision data.

DOI: 10.1103/PhysRevD.105.055028

I. INTRODUCTION

The Standard Model (SM) of particle physics has been proven to be remarkably successful in explaining most observations, starting from low-energy observables in weak decays to multiparticle production at the LHC. The last knot in the SM thread appears to be tied now, when it is established that the 125 GeV scalar discovered in 2012 is responsible (at least dominantly) in electroweak symmetry breaking and mass generation. Unfortunately, the SM is unable to account for the measured relic density, nonzero neutrino mass, baryon-antibaryon asymmetry, etc., along with aesthetic issues like fine-tuning in Higgs boson mass. It is a general consensus that it is a part of a more fundamental and complete theory which will be revealed to us at some higher energy scale. With the hope of testing the limitations of the SM, experimental results from the LHC have not revealed any hint of any such theory so far. However, the LHC is more than a particle discovery machine. We are entering an era of precision measurements as the high-luminosity run is close to its takeoff. Uncovering traces of new physics in the high-luminosity run is still a well-founded hope, if theoretical predictions can capture the deviation from SM with appropriate parametrization. It is in this spirit that effective operators are introduced, involving the SM fields. Such operators encapsulate contributions potentially arising from physics lying beyond the reach of direct searches, by modifying kinematical features of various final states especially in the high-energy tails. Therein lies the essential role of Standard Model effective field theory (SMEFT) [3–7].

In this formulation, it is assumed that if there is any new physics associated with the electroweak symmetry breaking sector the Higgs observed at the LHC is still a part of an $SU(2)_L$ doublet, the SM gauge invariance holds, and no additional light degrees of freedom relevant to the Higgs observables, are present in the spectrum. SMEFT interactions can be expressed as an operator expansion in inverse powers of a high energy scale, Λ,

$$\mathcal{L}_{\mathrm{SMEFT}} = \mathcal{L}_{\mathrm{SM}} + \sum_{i,n} \frac{C_i^{(n)}}{\Lambda^{n-4}} \mathcal{O}_i^{(n)} + \ldots \qquad (1)$$

Here, the leading-order term is the complete SM Lagrangian, and $\mathcal{O}_i^{(n)}$ are operators with mass dimension-n, constructed from the SM fields, and all of

*tibphy_rs@caluniv.ac.in
†adphys@caluniv.ac.in
‡biswarup@iiserkol.ac.in

the beyond the SM (BSM) physics effects reside in the coefficient $C_i^{(n)}$. The leading-order new physics effects that are associated with the effective field theory (EFT) operators, apart from a dimension-5 operator that contributes to neutrino masses, are of dimension 6. Neglecting flavor, there are 59 possible operators at dimension 6 [8,9].

At the LHC, the second most copious source for SM Higgs, next to the gluon fusion channel, is the vector boson fusion (VBF) mechanism [10]. This process has a rich kinematic structure with two forward tagging jets and little hadronic activity in the rapidity interval between them, resulting in clean samples of signal events and allowing for measuring the properties of Higgs with gauge bosons and fermions. Modifications from anomalous Higgs-gauge boson coupling (henceforth called HVV coupling) to VBF have been evaluated in Refs. [11–18]. Constraints on the higher-dimensional operators have been extensively studied on the basis of electroweak precision test and global fits of Higgs data in Refs. [19–25].

In this paper, we show that the dynamics of the forward tagging jets is sensitive to some additional effective interactions leading to Higgs boson production using the same final states as those studied for the VBF channel. We will critically look at the kinematic distributions of the tagging jets instead of looking for the Higgs decay products in the rapidity gap between two forward jets. We have used the $\gamma\gamma$ decay channel of the Higgs boson in our analysis. However, our main focus will be on the jet observables, and our method does not crucially depend on the Higgs decay modes. Consequently, other decay modes of Higgs (like $\tau^+\tau^-$, WW^*, etc.) can also be used in our analysis. When the contributions from all other channels are added, exclusion or discovery limits derived in our analysis are expected to improve further. The novelty of our study lies in the following points:

(1) Although the role of jet kinematics in VBF has been studied in earlier works [26–28], we point out some hitherto unexplored kinematic features which can play crucial roles in differentiating the effects of additional operators from those of SM-driven VBF, looking at the same final states. We illustrate this by using some higher-dimensional operators which accentuate this difference.

(2) The additional operators introduced here carry Lorentz structures that are distinct from the SM-induced one. The response of the event selection criteria are correspondingly different. We not only highlighted such difference but also attempted to utilise them in kinematic effects, by means of a correlated two-dimensional analysis between the geometric mean of the transverse momenta of the two forward jets produced in VBF and the rapidity difference between the two forward jets.

(3) Although it may have been noticed earlier, we underline the importance of bin-by-bin statistical significance in differential distributions, when it comes to distinguishing the additional dimension-6 operators, inducing new interactions of four-point vertices of the form $qqVH, (V = W^{\pm}, Z)$.

(4) We have duly estimated the next-to-leading-order (NLO) QCD corrections to VBF Higgs production in the presence of dimension-6 operators. The NLO QCD effect positively adds up to the leading-order (LO) rate without significantly affecting the overall shape of the kinematic distribution, albeit, improving the distinctness from the SM in most of the bins.

The outline of the paper is the following. In Sec. II, we review the basics of the effective field theory framework necessary for VBF Higgs production and discuss the motivation of this study followed by results of Monte Carlo study in Sec. III. In Sec. IV, the effects of new dimension-6 interactions are analyzed in the differential distributions of jet observables, by allowing one *nonzero* SMEFT coupling to vary at a time. We describe our phenomenological analyses in the VBF process by studying the sensitivity of these observables, along with the dependence on the LHC center-of-mass energy; our main findings are summarized in Sec. V.

II. OVERVIEW OF SMEFT OPERATORS RELEVANT FOR VBF HIGGS SIGNAL

We focus on the general set of dimension-6 gauge-invariant operators which give modifications in the VBF Higgs production. To facilitate our discussion, we present in Fig. 1 the Feynman diagrams, which, by virtue of SM interactions and dimension-6 effective operators, contribute to VBF amplitude. Black dots on some of the vertices of diagrams (b), (c), and (d) stand for possible inclusion of one of the higher-dimensional operators [4,8] listed below:

(i) The dimension-6 operators contain the SU(2) Higgs doublet φ and its derivatives:

$$\mathcal{O}_{H\Box} = (\varphi^\dagger\varphi)\Box(\varphi^\dagger\varphi);$$
$$\mathcal{O}_{HD} = (\varphi^\dagger D^\mu\varphi)^\star(\varphi^\dagger D_\mu\varphi). \quad (2)$$

These operators modify the SM Higgs couplings to other particles by multiplicative factors without bringing in any new Lorentz structure. This amounts to a renormalization of the Higgs field. Here, the covariant derivative D_μ has the usual meaning and contains $SU(2)_L$, $U(1)_Y$ gauge couplings and bosons.

(ii) The operators that induce fermion-fermion-gauge-Higgs ($qqVh$) or fermion-fermion-gauge (qqV) interactions leading to the amplitudes like (c) or (d) in VBF are

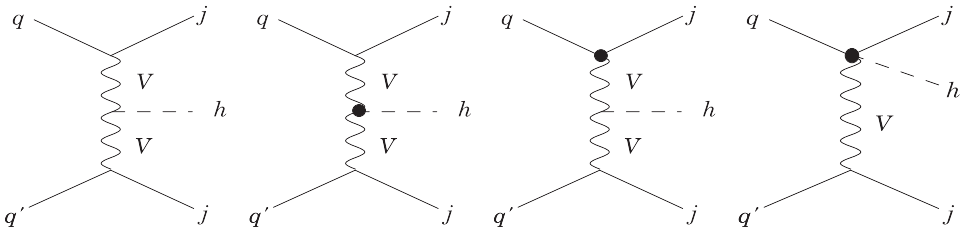

FIG. 1. Representative Feynman diagrams contributing to Higgs production via vector boson fusion topology. (a) is the SM process, while (b) and (c) processes involve the anomalous couplings of Higgs with gauge bosons and fermions, respectively. Diagram (d) involves the contact interaction between the Higgs, gauge boson, and fermions denoted with a blob.

$$\begin{aligned}
\mathcal{O}_{Hq}^{(1)} &= (\varphi^\dagger i\overleftrightarrow{D}_\mu \varphi)(\bar{q}_p \gamma^\mu q_r);\\
\mathcal{O}_{Hq}^{(3)} &= (\varphi^\dagger i\overleftrightarrow{D}^I_\mu \varphi)(\bar{q}_p \tau^I \gamma^\mu q_r)\\
\mathcal{O}_{Hu} &= (\varphi^\dagger i\overleftrightarrow{D}_\mu \varphi)(\bar{u}_p \gamma^\mu u_r);\\
\mathcal{O}_{Hd} &= (\varphi^\dagger i\overleftrightarrow{D}_\mu \varphi)(\bar{d}_p \gamma^\mu d_r)\\
\mathcal{O}_{Hud} &= i(\tilde{\varphi}^\dagger D_\mu \varphi)(\bar{u}_p \gamma^\mu d_r),
\end{aligned} \tag{3}$$

where we define $\varphi^\dagger i\overleftrightarrow{D}_\mu \varphi = \varphi^\dagger D_\mu \varphi - (D_\mu \varphi)^\dagger \varphi$ and $\varphi^\dagger i\overleftrightarrow{D}^I_\mu \varphi = \varphi^\dagger \tau^I D_\mu \varphi - (D_\mu \varphi)^\dagger \tau^I \varphi$. We use the notation of q for the quark doublet under $SU(2)_L$ and u, d for the $SU(2)$ singlet quarks, and p and r are generation indices.

Excepting the operator O_{Hud} (which induces a right-handed charged current), the VBF amplitudes constructed from any of these four operators $O_{Hq}^{(3)}$, $O_{Hq}^{(1)}$, O_{Hu}, and O_{Hd} interfere with the SM amplitude.

(iii) Another set of operators can induce $qqVh$ or qqV interactions. While their structure indicates that they are of magnetic dipole type and are different from the earlier ones, the presence of explicit dependence on the momentum of the gauge bosons in such operators due to the gauge field strengths will play a significant role in jet kinematics in which we are interested in this analysis:

$$\begin{aligned}
\mathcal{O}_{uW} &= (\bar{q}_p \sigma^{\mu\nu} u_r)\tau^I \tilde{\varphi} W^I_{\mu\nu};\\
\mathcal{O}_{dW} &= (\bar{q}_p \sigma^{\mu\nu} d_r)\tau^I \varphi W^I_{\mu\nu}\\
\mathcal{O}_{uB} &= (\bar{q}_p \sigma^{\mu\nu} u_r)\tilde{\varphi} B_{\mu\nu};\\
\mathcal{O}_{dB} &= (\bar{q}_p \sigma^{\mu\nu} d_r)\varphi B_{\mu\nu}.
\end{aligned} \tag{4}$$

Neglecting fermion masses, the dipole operators connect fermions of different helicities. Consequently, VBF amplitudes constructed out of such operators [Figs. 1(c) and 1(d)] do not interfere with the SM amplitudes.

(iv) Finally, there exist anomalous HVV interactions arising from the following set of dimension-6 operators [4,8]:

$$\begin{aligned}
\mathcal{O}_{HW} &= \varphi^\dagger \varphi W^I_{\mu\nu} W^{I\mu\nu}; \qquad \mathcal{O}_{HB} = \varphi^\dagger \varphi B_{\mu\nu} B^{\mu\nu};\\
\mathcal{O}_{HWB} &= \varphi^\dagger \tau^I \varphi W^I_{\mu\nu} B^{\mu\nu}.
\end{aligned} \tag{5}$$

These operators modify HVV couplings by introducing new Lorentz structure in the Lagrangian. Consequently, new VBF amplitudes [Fig. 1(b)] arising from such interactions add to the SM amplitude.

We present above a complete set of operators, which can modify the SM VBF Higgs signal. However, we illustrate our main points by using as samples the operators $\mathcal{O}_{Hq}^{(1)}$, $\mathcal{O}_{Hq}^{(3)}$, and $\mathcal{O}_{uW}$, and our study focuses on the important effect of differently structured interactions in the selection efficiencies and kinematic observables. Moreover, the method developed here is of general utility in studying all possible higher-dimensional operators. For instance, $\mathcal{O}_{fW}$ and $\mathcal{O}_{fB}$ operators differ in the cross section by a total factor $\tan^2\theta_W$. Also, as can be seen from the discussion of Fig. 2 in the following section, operators involving purely bosonic fields modify the VBF rates to a lesser extent than what fermionic operators do. We refer the reader to the discussion on Fig. 2 in the next section, which will hopefully clarify why these three operators can be treated as representative.

A comment about the numerical values of operator coefficients $\frac{C}{\Lambda^2}$, used in the following analysis, is relevant at this point. The ultimate guideline for the numerical values to be used lies in the available data from experiments. $\mathcal{O}_{Hq}^{(1)}$ and $\mathcal{O}_{Hq}^{(3)}$ lead to Z and W couplings to fermions with Lorentz structure similar to the SM. The electroweak precision measurements at LEP-I and LEP-II lead to stringent constraints on the Wilson coefficients of these operators. A global fit of electroweak observables to LEP data [29,30] leads to bounds on effective vector and axial-vector coupling of a pair of fermions to a Z boson, which

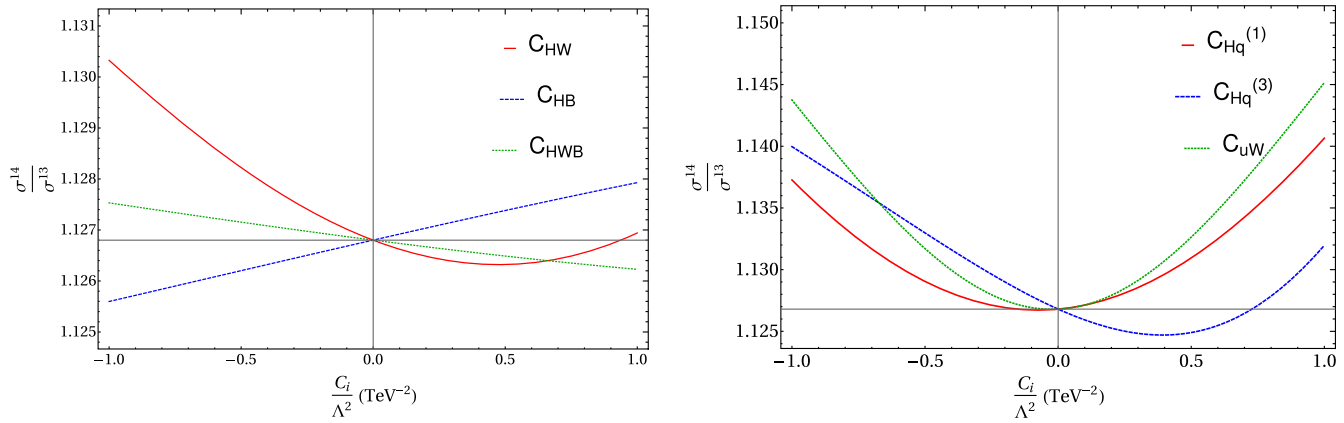

FIG. 2. Variation of ratio of cross sections at 14 and 13 TeV for $pp \to hjj(\to \gamma\gamma jj)$ with (a) C_{HW}, C_{HB}, C_{HWB} and (b) $C_{Hq}^{(1)}$, $C_{Hq}^{(3)}$, C_{uW}.

can be, in turn, translated into bounds at 95% C.L. on $|\frac{C_{Hq}^{(1,3)}}{\Lambda^2}|$, which is 1.11 TeV^{-2}. Similar constraints cannot be imposed on C_{uW} due to the chiral structure of $\mathcal{O}_{uW}$. However, one can think of imposing bounds on C_{uW} by considering its contribution to the anomalous magnetic moment of the u quark at tree level. But for the light quarks, $(g-2)$ is hard to extract in a model-independent way and is therefore subjected to large uncertainties [31].

Experimentally measured rates of nuclear beta decay as well as leptonic and semileptonic decays of pions and kaons and also constrain the couplings in which we are interested. For example, the allowed uncertainty of the pion form factor implies $\frac{|C_{Hq}^{(3)}|}{\Lambda^2} < 1.64$ TeV^{-2} at 90% C.L. [32].

TABLE I. 95% C.L. lower and upper limits (right column) on the relevant couplings $(\frac{C}{\Lambda^2})$ of selected dimension-6 operators (left column) obtained from comparing theoretical predictions with the combined ATLAS and CMS cross section measurements [33–36] from 13 TeV run of the LHC.

$Zh, h \to b\bar{b}$	95% C.L. allowed range
$\mathcal{O}_{Hq}^{(3)}$	$(-0.94, 0.41)$ (TeV^{-2})
$\mathcal{O}_{Hq}^{(1)}$	$(-0.72, 0.61)$ (TeV^{-2})
$\mathcal{O}_{uW}$	$(-0.68, 0.68)$ (TeV^{-2})
$Wh, h \to b\bar{b}$	95% C.L. allowed range
$\mathcal{O}_{Hq}^{(3)}$	$(-1.11, 0.43)$ (TeV^{-2})
$\mathcal{O}_{uW}$	$(-0.82, 0.82)$ (TeV^{-2})
$VBF, h \to \tau\bar{\tau}$	95% C.L. allowed range
$\mathcal{O}_{Hq}^{(1)}$	$(-5.4, 4.27)$ (TeV^{-2})
$\mathcal{O}_{Hq}^{(3)}$	$(-1.56, 3.7)$ (TeV^{-2})
$\mathcal{O}_{uW}$	$(-2.06, 2.06)$ (TeV^{-2})

The aforementioned operators are also subjected to the constraints imposed by the LHC data. In Table I, we have listed the bounds taking one operator at a time, obtained by comparing the expected cross section with experimental data from ATLAS and CMS collaborations [33–36].

The most stringent limits on $\frac{C_{Hq}^{(3)}}{\Lambda^2}$, $\frac{C_{Hq}^{(1)}}{\Lambda^2}$, and $\frac{C_{uW}}{\Lambda^2}$ arise from the measured cross section, of associated production of Higgs with a vector boson (Vh production) because of higher accuracy in its measurement.

As already mentioned, $\mathcal{O}_{H\Box}$ and $\mathcal{O}_{HD}$ will renormalize the Higgs wave function, and in turn, it will modify all the Higgs observables. We have obtained bounds on these two operators by comparing the Higgs production rate via VBF with ATLAS data [35]. The 95% confidence intervals for these couplings are listed in the Table II. However, this set of operators will not give us Higgs couplings to other SM particles with new Lorentz structure and will only rescale the Higgs interactions. These contributions, thus, not changing the momentum structures of the vertices involved, are of limited interest to investigate the effects of such operators any further, in our study.

Some theoretical considerations are also important, and we now pay some attention to these. A guiding principle is a good high-energy behavior of the scattering amplitudes on the inclusion of higher-dimensional operators involving such coupling. The scattering amplitudes constructed out of such effective operators must satisfy the unitarity bound, namely, $|\mathcal{R}e\, a_0| < 0.5$, where a_0 is the lowest partial wave

TABLE II. 95% C.L. allowed range (right column) on the relevant couplings $(\frac{C}{\Lambda^2})$ of selected dimension-6 operators (left column) obtained from comparing theoretical predictions with ATLAS [35] from the 13 TeV run of the LHC.

$\mathcal{O}_{H\Box}$	$(-41.24, 8.28)$ (TeV^{-2})
$\mathcal{O}_{HD}$	$(-17.57, 25.4)$ (TeV^{-2})

amplitude. The violation of unitarity appears at energies of a few TeV for the values of Wilson coefficients allowed by the Higgs data, with the exact value depending upon the specific choice of operators and the process under consideration. A simplified unitarity analysis $q\bar{q} \to Vh$ leads to an upper bound of 2.82, 8.81, and 1.41 TeV^{-2} on $|\frac{C_{Hq}^{(3)}}{\Lambda^2}|$, $|\frac{C_{Hq}^{(1)}}{\Lambda^2}|$, and $|\frac{C_{uW}}{\Lambda^2}|$, respectively, assuming an incoming parton inside a proton carries typically 1 TeV of energy at the LHC.

In the subsequent study, keeping such constraints in mind, the effective coupling strengths need to be consistent with the electroweak data, partial wave unitarity, and the Higgs measurements. Within such constraints, we concentrate on the effective operators $\mathcal{O}_{Hq}^{(1)}$, $\mathcal{O}_{Hq}^{(3)}$, and $\mathcal{O}_{uW}$ and examine their role in modifying the VBF rates. The following sections contain a description of our strategy and results.

III. COLLIDER ANALYSIS

We implemented the effective Lagrangian of SMEFT in FeynRules [37]. MadGraph-5 [38] has been used to generate parton-level events. The SM cross sections have been estimated at the NLO as implemented in MadGraph-5. While generating events driven by new physics, we assume that only LO SMEFT contribution is absorbed within the Wilson coefficient of the dimension-6 operators. We use the NNPDF23NLO parton distribution function [39] with renormalization and factorization scale equal to half the Higgs mass ($\mu_R = \mu_F = \frac{m_H}{2}$). We also checked that the results with other scale choice (viz., at the scalar sum of transverse momentum of all final-state products) do not differ by more than 5%. The $pp \to h(\to \gamma\gamma)jj$ is generated at $\sqrt{s} = 14$ TeV. The events are passed through PYTHIA 8 [40] for parton showering and hadronization. We performed the detector simulation in DELPHES [41] for analyzing the hadron-level events. The jets are reconstructed by following the anti-k$_t$ algorithm using FASTJET [42].

We start by reminding the reader that we would like to investigate how the VBF Higgs signal gets modified in the presence of new dimension-6 operators. To present our case, we confine to the diphoton decay channel of the Higgs boson. To validate our analysis, we applied the ATLAS [43] cut flow listed in Table III, described in Ref. [44], to the SM VBF Higgs production followed by its diphoton decay. As a preselection requirement, we selected events with photons with minimum transverse momentum of 25 GeV, within $|\eta| < 2.37$ and separated from each other with $\Delta R > 0.4$. The jets are reconstructed with radius parameter 0.4 with minimum 30 GeV transverse momentum and within $|\eta| < 4.5$. Note that the cuts as listed in Table III are optimized to keep out the background to VBF in the form of Higgs production via gluon production along with two jets and also non-Higgs backgrounds.

TABLE III. Relative efficiencies of each of the experimental cuts and the expected number of events for the signal cross section in the $H \to \gamma\gamma$ channel, for the Higgs production via vector boson fusion, for an integrated luminosity of 3000 fb^{-1} at the 14 TeV LHC.

Cut	Ref. [44] efficiency	Our MC efficiency	Events
Preselection	...	...	15841
$N_{\text{jets}} \geq 2$	0.838	0.852	13497
$N_{b-\text{jet}} = 0$	0.968	0.997	13456
$\lvert\Delta\eta_{jj}\rvert > 3$	0.756	0.798	10738
$\eta_{j_1} \cdot \eta_{j_2} < 0$	0.987	0.982	10545
$M_{jj} > 600$ (GeV)	0.796	0.846	8921
$N_\gamma = 2$	0.657	0.612	5459
$I_\gamma^{R=0.4} < 15\%$	0.998	0.996	5438
$\Delta R_{\gamma j}^{\min} > 1.5$	0.886	0.823	4475
$\lvert\Delta\Phi_{\gamma\gamma,jj}\rvert > 1.5$	0.976	0.953	4265
$\Delta\Phi_{j_1,j_2} < 2$	0.610	0.583	2486
$122 < M_{\gamma\gamma} < 128$ (GeV)	0.996	0.998	2481
$y_{j_{1,2}}^{\min} < y_h < y_{j_{1,2}}^{\max}$	0.984	0.977	2424

The net efficiency of our selection cuts (0.153) agree with Ref. [44] (0.163) rather closely. The purpose of this exercise is overall validation of our MC, so we can extract the efficiencies of the same cut flow when dimension-6 SMEFT operators are included within our own setup.

As already mentioned in the previous section, several operators can modify the SM VBF Higgs signal. The total rates and their ratios at two different center-of-mass energies can uncover signatures of the new and anomalous couplings of Higgs to other SM particles. In general, the energy dependence of the rates can be sensitive to the effective operators. We study now, the ratio of VBF Higgs cross sections at 14 and 13 TeV (at the LHC), keeping one of the aforementioned dimension-6 operators nonzero at a time along with the SM. The Higgs production cross section is expected to be more sensitive to the energy of collision in the presence of any of the higher-dimensional operators than in the situation when production dynamics is solely controlled by the SM.

The variations of the ratios of the cross section at the LHC center-of-mass energy at 14 to 13 TeV are presented in Fig. 2(a) and 2(b), respectively, with varying Wilson coefficient values of various dimension-6 operators. The effects of the different operators to show up to different degrees in such a ratio. A gray line (corresponding to the value of the ratio of 1.268) parallel to the x axis in both the plots represents the SM case, where the relative enhancement of the cross section is mainly due to parton flux evaluated at 14 TeV *vis-à-vis* that at 13 TeV.

A look into Fig. 2(a) reveals that the bosonic operators ($\mathcal{O}_{HW}$, $\mathcal{O}_{HB}$, and $\mathcal{O}_{HWB}$) have a mild effect on the VBF Higgs cross section in contributing to the SM. For values of

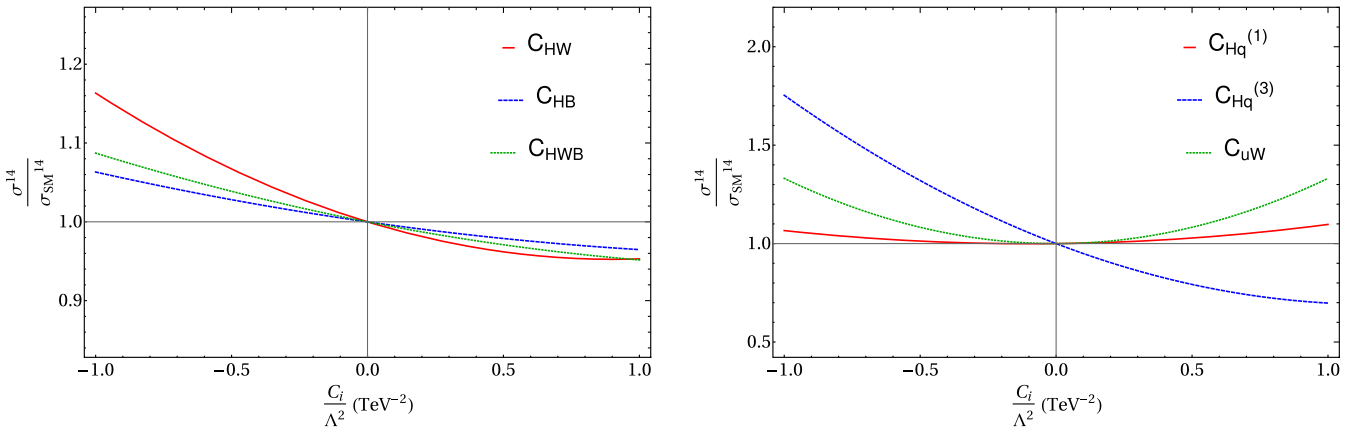

FIG. 3. Variation of ratio of cross sections of VBF Higgs production in presence of dimension-6 operators to the SM cross section of the same at 14 TeV with (a) C_{HW}, C_{HB}, C_{HWB} and (b) $C_{Hq}^{(1)}$, $C_{Hq}^{(3)}$, C_{uW}.

C_i/Λ^2 varying in the range $[-1:0]$ TeV^{-2}, the deviation of the ratio from its SM value is the least for $\mathcal{O}_{Hq}^{(1)}$ in comparison to other two fermionic operators as shown in Fig. 2(b). In the same range of values of C_i/Λ^2, the $\mathcal{O}_{HW}$-driven ratio would deviate the most, from its SM value, in comparison to two other bosonic operators, $\mathcal{O}_{HB}$ and $\mathcal{O}_{HWB}$. However, the C_{HW}-driven ratio is less pronounced everywhere in this range of C_i/Λ^2 than the $C_{Hq}^{(1)}$-driven ratio. The ratio changes by 0.92% for $C_{Hq}^{(1)}$, whereas for C_{HW}, it changes by 0.32% for C_i/Λ^2 in the range $[-1:0]$ TeV^{-2}. Similarly, for positive values of Wilson coefficients, the C_{HB}-driven ratio deviates the most from the SM value, and in the same range, the least deviation occurs due to $\mathcal{O}_{Hq}^{(3)}$. However, the latter is greater in magnitude than the C_{HB}-driven ratio in the range $[0:1]$ TeV^{-2}. In a nutshell, for a given value of $\frac{C}{\Lambda^2}$, any of the dimension-6 operators involving the interaction of quarks, gauge, and Higgs can modify the SM cross section more than any of the operators involving anomalous coupling of bosons and Higgs only. Henceforth, we will only investigate the effects of $\mathcal{O}_{Hq}^{(1)}$, $\mathcal{O}_{Hq}^{(3)}$, and $\mathcal{O}_{uW}$, from the aforementioned groups of dimension-6 operators as they modify the VBF cross section the most.

We have also estimated the strength of VBF Higgs production cross section for different values of effective couplings normalized to the SM cross section. Our finding on which operator gives the maximum effect remains unchanged. In Fig. 3, the variations of cross section ratios are presented. One can easily see from Fig. 3 that in case of the operators involving two fermions a gauge boson and a Higgs (right panel) difference of the ratios from unity are more pronounced than the cases involving the bosonic operators (left panel).

The enhancement of cross section in case of dimension-6 operators involving fermions can be accounted for by the absence of an extra propagator which is present in the SM-like VBF processes involving the bosonic operators. Most of the high-energy contribution due to these operators has an amplitude that is distinct from the SM contribution because of a quadratic growth with respect to the Mandelstam variable t.

A comment is in order here. Two of our operators ($\mathcal{O}_{Hq}^{(1)}$ and $\mathcal{O}_{Hq}^{(3)}$) do interfere with the SM contributions, while $\mathcal{O}_{uW}$ does not. One thus expects new contributions proportional to both $\frac{1}{\Lambda^2}$ and $\frac{1}{\Lambda^4}$. While it is expected in a general study to include all the contributions in a given order $(\frac{1}{\Lambda^2}, \frac{1}{\Lambda^4})$, we are illustrating our points in the context of a simplified scenario when one new operator arises at a time. The discussion otherwise becomes so nontransparent and unwieldy that our main emphasis, namely, the influence of the differently structured operators on jet kinematics, is lost. In the same spirit, when we are considering contributions up to quadratic order, $(\mathcal{O} \sim \frac{1}{\Lambda^4})$, we have neglected the existence of additional dimension-8 operators which could participate at the same order. We reiterate that such simplemindedness gives us the chance to explore the physical content of each operator.

The dependence of the efficiency (of the cuts)[1] on a particular Wilson coefficient will largely be controlled by interference with SM amplitudes. This feature will be more clearly revealed if the efficiency of the cuts (listed in Table III) is parametrized as a function of the Wilson coefficients.

[1]The efficiency as a function of the parameters C_i is defined as $\epsilon_{\gamma\gamma+2\text{-jets}}(C_i) = \frac{[\sigma(pp\to Hqq\to\gamma\gamma jj)]^{\text{VBF}}_{\text{After Cuts}}}{[\sigma(pp\to Hqq\to\gamma\gamma jj)]^{\text{VBF}}_{\text{Before Cuts}}}$.

Efficiencies are found to be second-order polynomial functions of the Wilson coefficients. We calculate the total cross section in the presence of higher-dimensional operators at LO, in corroborating the fact that any higher-order correction can affect the dependence of the cross section on the coefficient of dimension-6 operators nontrivially [45,46]. Each power of coefficient C_i is suppressed by Λ^2. For various choices of this cutoff scale Λ, the coefficients will be scaled according to the power of C_i involved. We have neglected any contribution from dimension-8 operators to the signal. The error due to this truncation at dimension-6 level cannot be estimated in a model-independent way [47].

The efficiency corresponding to each of the coefficients C_i can be expressed as

$$\begin{aligned}
&\epsilon_{\gamma\gamma+2-\text{jets(VBF)}}(C_{Hq}^{(1)}) \\
&= \frac{(0.6553 + \frac{C_{Hq}^{(1)}}{\Lambda^2}0.02327 + \left(\frac{C_{Hq}^{(1)}}{\Lambda^2}\right)^2 0.04144)}{(4.26 + \frac{C_{Hq}^{(1)}}{\Lambda^2}0.1905 + \left(\frac{C_{Hq}^{(1)}}{\Lambda^2}\right)^2 0.3462)}, \\
&\epsilon_{\gamma\gamma+2-\text{jets(VBF)}}(C_{Hq}^{(3)}) \\
&= \frac{(0.6553 - \frac{C_{Hq}^{(3)}}{\Lambda^2}0.3808 + \left(\frac{C_{Hq}^{(3)}}{\Lambda^2}\right)^2 0.16604)}{(4.26 - \frac{C_{Hq}^{(3)}}{\Lambda^2}2.373 + \left(\frac{C_{Hq}^{(3)}}{\Lambda^2}\right)^2 1.347)}, \\
&\epsilon_{\gamma\gamma+2-\text{jets(VBF)}}(C_{uW}) \\
&= \frac{(0.6553 + (\frac{C_{uW}}{\Lambda^2})^2 0.27)}{(4.26 + (\frac{C_{uW}}{\Lambda^2})^2 2.76)},
\end{aligned} \tag{6}$$

where the coefficients $\frac{C_i}{\Lambda^2}$ are in units of TeV^{-2}.

Some clarification is in order at this stage. The quantities of the form $\frac{C_i}{\Lambda^2}$ are intrinsically dimensionful; therefore, $|\frac{C_i}{\Lambda^2}| \simeq 1$ in this unit does not necessarily imply a breakdown of the EFT expansion. It means that the UV completion of our effective Lagrangian is a strongly coupled theory for large Λ, while for relatively small Λ, it entails a weak UV completion. Furthermore, for example, in the first line of Eq. (6), the term proportional to the square of $\frac{C_{Hq}^{(1)}}{\Lambda^2}$ exceeds the interference term in this limit, which may raise questions about the validity of the EFT expansion. However, such a doubt is dispelled, so long as the interference of the subsequent dimension-8 terms with the SM amplitude remains smaller than the aforementioned quadratic terms. It may be legitimately expected that such an interference term is indeed smaller due to the occurrence of g_{SM}^2 in it, so long as the energy dependence of the Wilson coefficients in the dimension-8 terms is similar to that in the dimension-6 square terms [18,47]. This hopefully conveys an idea about the scope of Eq. (6).

In Fig. 4, we show how efficiency depends on the Wilson coefficients, $C_{Hq}^{(1)}$, $C_{Hq}^{(3)}$, and C_{uW}. A small range of C_i $(|\frac{C_i}{\Lambda^2}| < 1\ \text{TeV}^{-2})$ consistent with unitarity and LEP limits has been used in these plots for illustration. We recover the SM efficiency $\epsilon_{\text{SM}} \simeq 0.153$, for zero values of these couplings. A symmetric nature of the green curve corresponding to C_{uW} reveals the noninterfering nature of corresponding operator, $\mathcal{O}_{uW}$ with the SM. Here, the $\mathcal{O}(\frac{1}{\Lambda^4})$ term in the cross section contains the leading BSM effect. The other two, namely, $\mathcal{O}_{Hq}^{(1)}$ and $\mathcal{O}_{Hq}^{(3)}$, do interfere with SM amplitudes, albeit differently, which can be easily realized by the presence of a positive (negative) sign in front of linear (in C_i) terms in the expressions of efficiencies in Eq. (6). The linear dependence of the cross section on $C_{Hq}^{(3)}$ is more sensitive than that on $C_{Hq}^{(1)}$; however, including the full amplitude squared guarantees it to be positive definite and would facilitate distinguishing it from the SM. A naive scaling of the SM coupling alone by a multiplicative factor does not change of efficiency of cuts.

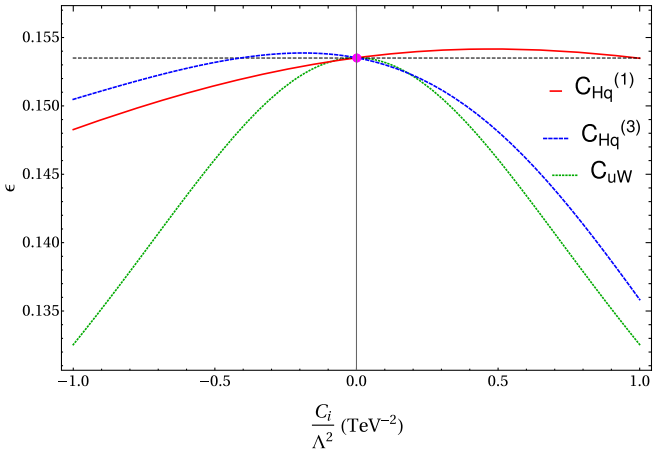

FIG. 4. Efficiency of VBF cuts (ϵ) as a function of $\frac{C_i}{\Lambda^2}$ in the $h \to \gamma\gamma$ channel at 14 TeV.

The efficiency as a function of $\frac{C_i}{\Lambda^2}$ alone gives us limited information about how much an operator can modify the VBF Higgs cross section from its SM value. The acceptance of these operators is not the same in the same regions of phase space, and we must take into account the total and differential cross section along with the efficiency to predict the above modification.

We are now ready to investigate how the chosen dimension-6 operators may affect the various kinematic distributions. Our emphasis will be on those kinematic variables which can be constructed out of the 4-momenta of tagging jets. Our aim is to extract maximum information from the jet observables without looking at the Higgs boson decay products so that the strategy followed in this article could be used for any other decay channels of Higgs boson produced via the VBF mechanism.

In the following, we will illustrate few of them in which we find the new physics effect is prominent. A value of $\frac{C}{\Lambda^2} = 0.3\ \text{TeV}^{-2}$ has been used in these distributions.

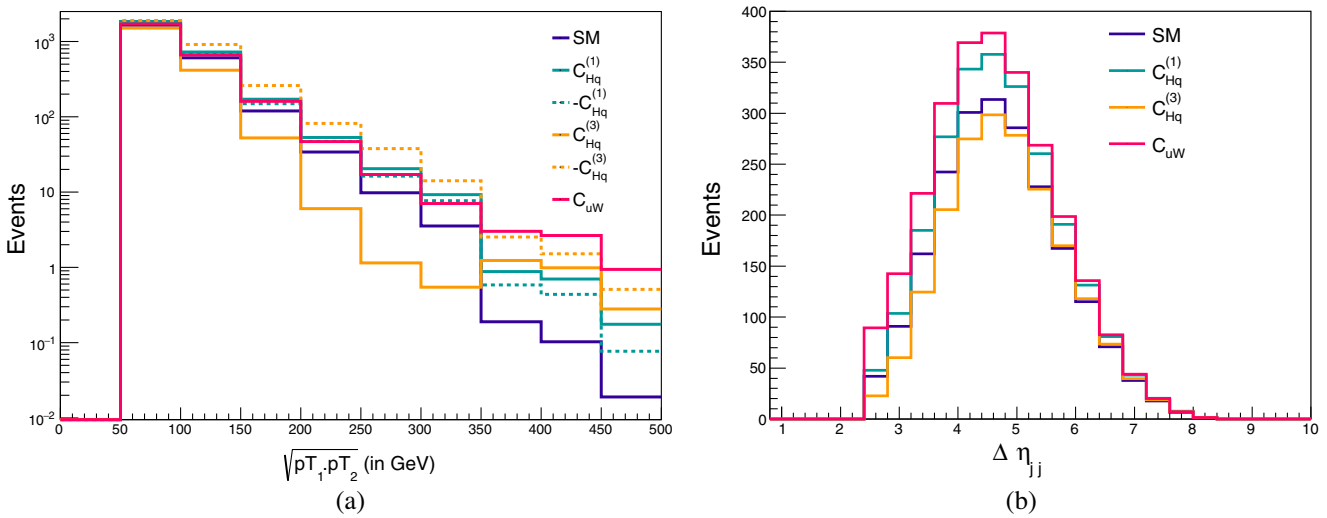

FIG. 5. (a) p_{T12}, geometric mean of leading jet p_Ts and (b) $\Delta\eta_{jj}$, rapidity separation between leading jet pair distributions, in SM and SMEFT. The differential distribution of events are presented with 3000 fb^{-1} data at 14 TeV LHC. For the EFT predictions, we have chosen $\frac{C_{Hq}^{(1)}}{\Lambda^2} = 0.3$ TeV^{-2} (green, solid), $\frac{C_{Hq}^{(3)}}{\Lambda^2} = 0.3$ TeV^{-2} (yellow, solid), and $\frac{C_{uW}}{\Lambda^2} = 0.3$ TeV^{-2} (red, solid). The dashed lines in (a) represent the same values of the respective Wilson coefficients but with negative signs.

The foremost is the geometric mean of p_T of forward jets, $p_{T12}(\equiv\sqrt{p_{T1}p_{T2}})$ distribution[2] as shown in Fig. 5(a). Sensitivity to dimension-6 operators is more pronounced at the tails of p_{T12} of the jets when we compare them with the SM. A few important aspects of this distribution are worth noting:

(i) Both $\mathcal{O}_{Hq}^{(1)}$ and $\mathcal{O}_{Hq}^{(3)}$ interfere with the SM amplitude. The solid lines correspond to positive values of Wilson coefficients. The corresponding dashed lines correspond to negative values of the coefficients. The former (green solid line) enhances the event population steadily with increasing bins of p_{T12} with respect to the SM (blue line). However, the absolute value for the excess events from the SM keeps on decreasing.

(ii) The operator $\mathcal{O}_{Hq}^{(3)}$ (yellow line) has destructive interference with SM, which is evident from the suppression of number of events in moderately low p_{T12} bins (< 350 GeV) in comparison to the SM, while for p_{T12} bins (>350 GeV), there is substantial contribution due to the quadratic contribution of this operator in this region of phase space, relative to the destructive interference. The sign of the Wilson coefficient $C_{Hq}^{(3)}$ does not affect the hardness of the distribution in these regions as is noticeable from the distribution corresponding to negative value of the EFT coupling.

(iii) $\mathcal{O}_{uW}$ does not interfere with the SM. The presence of an explicit momentum (of the weak gauge boson) in the coupling helps in producing a higher number of jets with high p_T.

(iv) If a negative departure from the SM is observed in the measured p_{T12} (or p_T) distribution(s) of the leading forward jets in VBF events, that not only points toward a new interaction but also ensures a specific form of new physics, e.g., either $\mathcal{O}_{Hq}^{(1)}$ or $\mathcal{O}_{Hq}^{(3)}$.

Next, we look at the distribution of rapidity separation of the forward jet pair [Fig. 5(b)]. The shapes of the distributions are similar, however, with different normalizations due to the interfering or noninterfering nature of the corresponding dimension-6 operators. Nevertheless, a careful look at this plot reveals that events with smaller $\Delta\eta_{jj}$ (< 4) are mostly generated by these higher-dimensional operators, which implies that the events originating from new physics are characterized with two forward jets with smaller rapidity separation at least for the operators $\mathcal{O}_{Hq}^{(1)}$ and $\mathcal{O}_{uW}$. This observation, in association with the fact that new physics events appear with high p_T jets, can help us in separating the new physics rich phase-space region from the SM. We demonstrate the correlation between two variables $\Delta\eta_{jj}$ and p_{T12} in Fig. 6, in which it is found that the populated regions in the $p_{T12} - \Delta\eta_{jj}$ space display a shift when the new physics effects due to higher-dimensional operators are included.

Before we delve into a discussion of such a correlation between $\Delta\eta_{jj}$ and p_{T12}, let us comment on the method that we have followed to obtain such a distribution. Although

[2]In the presence of dimension-6 operators, both the forward jets have higher p_T compared to the SM case. To capture this enhancement in one distribution, we choose p_{T12} instead of individual p_T of the tagging jets.

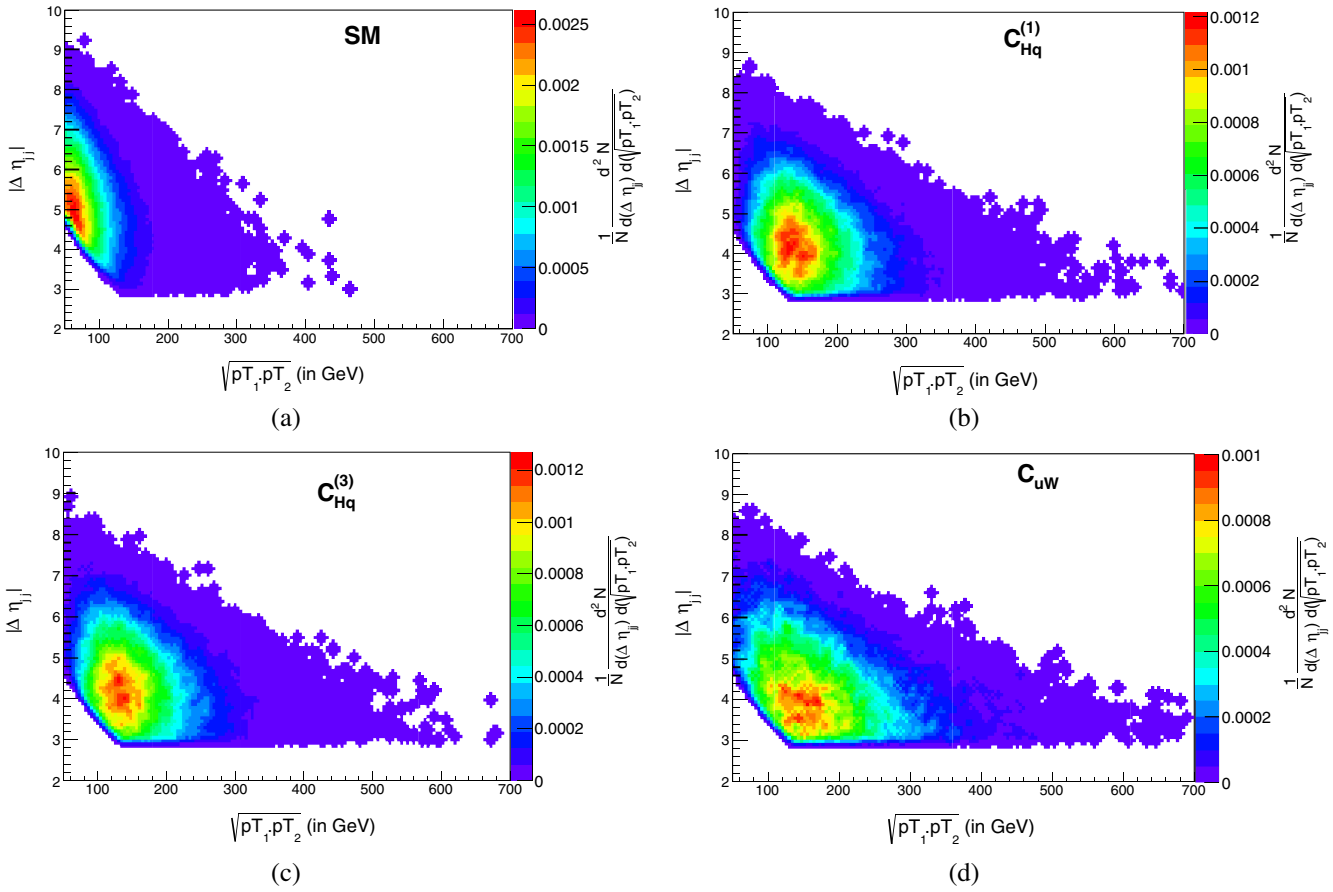

FIG. 6. Two-dimensional histograms showing the correlation of the rapidity gap of jets $\Delta\eta_{jj}$ with p_{T12}, the geometric mean of p_T of two leading jets at $\sqrt{s} = 14$ TeV. The z axis indicates the normalized frequency of events, in arbitrary units. The SM contributions in the absence of dimension-6 interactions have been subtracted in (b), (c), and (d). $\frac{C}{\Lambda^2} = 0.3$ TeV^{-2} has been assumed in (b), (c), and (d).

new physics effects are visible in the p_{T12} distributions of the tagging forward jets, for high p_{T12} values [see Fig. 5 (a)], the difference between the SM and new physics is not prominent in the distribution of rapidity separation between the jets [see Fig. 5(b)]. Because of a large cross section of VBF Higgs production in the SM, any small modification due to the dimension-6 SMEFT operators, in the shape of kinematic distributions, becomes less distinct, particularly in the $\Delta\eta_{jj}$ plot. It is these small relative differences between the EFT and the SM predictions that we are interested in, as they drive the sensitivity of new physics. Therefore, to highlight any modification due to these new interactions, we have subtracted, bin by bin, the number of events predicted purely by the SM from the total number of events obtained in the presence of any of the aforementioned dimension-6 operators along with SM. We study the regions satisfying this criterion [48]. Experimentally, this amounts to subtracting the purely SM prediction from the experimental data, an exercise that is reasonably reliable in view of the extensive studies on SM contribution to VBF. The effect of this subtraction is evident as one can see the different position of peaks (red regions) of the two-dimensional histograms.

Some salient features of such a double differential distribution are as follows:

(i) The region with moderate p_{T12} ranging from 50 to 400 GeV (with mean value at 100 GeV) and $\Delta\eta_{jj}$ around 5.2 (red color indicates larger larger number of events) is mostly populated by SM VBF-Higgs events. The central region is depleted of any hadronic activity due to the color singlet (in this case electroweak gauge bosons) exchange in the t channel.

(ii) Regions with high values of (>100 GeV and extending up to 700 GeV) and relatively smaller rapidity gaps ($\Delta\eta_{jj} \leq 4$) are populated by the new physics events.

(iii) These new vertices tend to push p_T of jets to higher values and these hard jets are at small $\Delta\eta_{jj}$ gap compared to SM. Such a correlation is most prominent for C_{uW}, which have $|\Delta\eta_{jj}|$ distribution peaking around 4. The effects of other two operators, too, extend to jet-p_T values as high as 700 GeV. We urge the experimentalists to revisit the VBF data and ascertain or rule out the presence of events in the above region in the $p_{T12} - \Delta\eta_{jj}$ plane.

IV. SENSITIVITY OF THE VBF SIGNAL TO NEW INTERACTIONS

We are now ready to quantify the sensitivity of VBF Higgs signal to the Wilson coefficients of the higher-dimensional operators that we have been using in our discussion. We calculated the projected significance in the vector boson fusion channel for illustrative values of $\frac{C_i}{\Lambda^2}$, for 14 TeV LHC at 3000 fb^{-1} luminosity. The significance $\mathcal{Z}$ [49] is defined as follows:

$$\mathcal{Z} = \sqrt{2\left[(S+B)\mathrm{Log}\left(1+\frac{S}{B}\right)-S\right]} \tag{7}$$

Signal (S) is defined as $S = |N^H_{\mathrm{BSM}} - N^H_{\mathrm{SM}}|$. Here, N is the number of events for a given time integrated luminosity. We emphasize that generation of our signal events comprises all the topologies (driven by the SM and EFT couplings) leading to the $pp \to h(\to \gamma\gamma)jj$ final states. Such final-state topologies can arise from Higgs production via VBF, in association with a W/Z or via gluon fusion process. Although these processes may interfere, the invariant mass of the two leading jets is itself a powerful discriminating variable that permits us to exclusively select final states arising from the VBF mechanism. The quantity B is defined as $N^H_{\mathrm{SM}} + N^{\mathrm{NH}}_{\mathrm{SM}}$. $N^H_{\mathrm{BSM(SM)}}$ in our signal consists of the number of VBF Higgs events in the SM. We have also included, in the VBF-enriched phase space, the number of SM Higgs events produced via the gluon fusion channel and Vh channel that are allowed by VBF selection cuts, and finally, $N^{\mathrm{NH}}_{\mathrm{SM}}$ is the number of non-Higgs events (leading to the same final state with two photons and two jets) in the SM[3] allowed by the VBF selection cuts.

Higgs boson production via gluon fusion (ggF) and in association with a W/Z also contaminates the VBF-Higgs cross section. The rate of production of a Higgs boson via ggF and passing through VBF selection criteria is estimated to be 30% [50] of the true VBF Higgs cross section. To optimize our event rates, we impose a cut on rapidity gap between the tagged forward jets of 3 instead of 4 and an invariant mass of at least 600 GeV for the tagged forward jet pair, instead of 400 GeV used in Ref. [50]. We assume Higgs production cross section due to ggF passing through VBF selection criteria is 40% that of true VBF cross section. Higgs boson production in association with a Z or W bosons can also contribute to VBF signal. However, a demand of high invariant mass ($M_{jj} > 600$ GeV) of a pair of jets appearing in the opposite hemisphere ($\eta_1\eta_2 < 0$) controls this background. Finally, we add another 40% of the true VBF cross section to background (B) to also take into account the SM contribution from non-Higgs events producing photons and jets passing VBF selection cuts. One, thus, arrives at 815 background events at 3000 fb^{-1}, which is larger than the expected background estimates of 780 events at 3000 fb^{-1} in Ref. [44]. Therefore, if we have made an error, it is on the conservative side.

[3]The non-Higgs backgrounds consist of nonresonant production of a diphoton, a single photon, and fake photons in association with more than one jet.

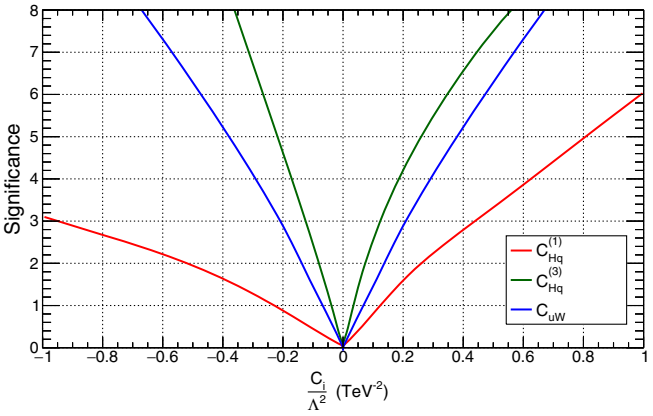

FIG. 7. Significance $\mathcal{Z}$ (calculated using total cross sections) as a function of $\frac{C_i}{\Lambda^2}$ at $\sqrt{s} = 14$ TeV, 3000 fb^{-1} for $pp \to h(\to \gamma\gamma)jj$.

To see how sensitive $\mathcal{Z}$ is to the Wilson coefficients, we estimate $\mathcal{Z}$, in two different ways. The first one of them is by plugging into Eq. (7) the total cross sections of signal and background subjected to the cuts. In addition, we calculate $\mathcal{Z}$, by comparing signal strength with background in bins of p_{T12}. In the following, both the results along with their implication will be presented.

In Fig. 7, we present the variation of $\mathcal{Z}$ with $\frac{C_i}{\Lambda^2}$ for an integrated luminosity of 3000 fb^{-1}. The key features emerging from Fig. 7 are as follows:

(i) Of all operators that we have considered, $\mathcal{O}^{(3)}_{Hq}$ can modify the SM cross section the most. Negative values of the Wilson coefficients of $\mathcal{O}^{(3)}_{Hq}$ increase the cross section from its SM prediction more than the positive values. A 3σ signal significance over the background can be achieved even for small values of $\frac{C^{(3)}_{Hq}}{\Lambda^2} \in (-0.13, 0.14)$ TeV^{-2}.

(ii) The operator $\mathcal{O}^{(1)}_{Hq}$ involves a left-handed charged current of fermions with a weak gauge boson and Higgs. The positive values of Wilson coefficients of this operator enhance the cross section more than negative coupling strength. Signal stands over the background at 3σ level for $\frac{C_i}{\Lambda^2} \simeq 0.45$ TeV^{-2}, whereas, for $\frac{C_i}{\Lambda^2} \simeq -0.8$ TeV^{-2}, the 2.6σ effect can be barely achieved.

(iii) The dipole operator $\mathcal{O}_{uW}$ along with the SM results in the largest cross section of all three operators that we have considered. Despite having the lowest selection efficiency, the cross section is large enough for signal to stand against the background with 3σ significance for $|\frac{C_i}{\Lambda^2}| > 0.22$ TeV^{-2}.

TABLE IV. Variation of signal significance, $\mathcal{Z}$ [calculated using Eq. (7) along the bins of p_{T12} of the tagging forward jet pair with *positive* and *negative* values of Wilson coefficients.

Bin (GeV)	$\frac{C_{Hq}^{(1)}}{\Lambda^2} = 0.3(-0.3)$ TeV^{-2}	$\frac{C_{Hq}^{(3)}}{\Lambda^2} = 0.3(-0.3)$ TeV^{-2}	$\frac{C_{uW}}{\Lambda^2} = 0.3(-0.3)$ TeV^{-2}
150–200	3.57 (2.01)	5.35 (9.03)	2.61
200–250	2.43 (1.67)	4.07 (7.0)	3.32
250–300	2.28 (1.32)	3.68 (4.7)	4.19
300–350	1.65 (1.09)	2.45 (3.84)	4.45
350–400	1.54 (0.92)	2.57 (3.35)	5.53
400–450	1.39 (0.78)	2.15 (3.18)	5.95
450–500	1.24 (0.49)	1.94 (2.65)	6.32

(iv) Figure 7 reveals $|\frac{C_{Hq}^{(3)}}{\Lambda^2}| < 0.14$ TeV^{-2}, which seems to be a clear improvement over the limit derived on the same coupling from LEP electroweak data and Higgs data. Similar but less improvement of limits has been observed in the case of $\frac{C_{Hq}^{(1)}}{\Lambda^2}$. $\frac{C_{uW}}{\Lambda^2}$ could not be constrained from LEP bounds.

Now, we turn to the calculation of $\mathcal{Z}$ in the bins of p_{T12}. Looking at the p_{T12} distributions [in Fig. 5(a)], one can see that the signal stands above the background in individual bins (of p_{T12}) spanning over a wide range of its value. One can calculate the significance of signal in individual bins to gather maximum information from the kinematics of the forward jets. We present in Table IV, how the signal significance changes along the bins of p_{T12} with different dimension-6 operators with the values of their Wilson coefficients set equal to 0.3 TeV^{-2} with an integrated luminosity of 3000 fb^{-1}. The values of $\mathcal{Z}$, in the same bins of p_{T12}, are also presented in the same table, with $\frac{C}{\Lambda^2} \simeq -0.3$ TeV^{-2}. Such values of $\mathcal{Z}$ will help us understand the effect of interference of new physics with the SM.

The following points emerge from Table IV:

(i) For $\mathcal{O}_{Hq}^{(1)}$ and $\mathcal{O}_{Hq}^{(3)}$, nonsymmetric cut efficiencies as a function of $\frac{C}{\Lambda^2}$ (see Fig. 4) lead to the significance, $\mathcal{Z}$, having different sensitivity to positive and negative values of $\frac{C}{\Lambda^2}$. For example, the operator $\mathcal{O}_{Hq}^{(3)}$ which interferes destructively with the SM signal significance improves appreciably while calculated with $C_{Hq}^{(3)}/\text{TeV}^{-2} < 0$ in comparison to its values calculated with $C_{Hq}^{(3)}/\text{TeV}^{-2} > 0$, whereas for a constructively interfering operator $\mathcal{O}_{Hq}^{(1)}$, a higher signal significance can be achieved always with $C_{Hq}^{(1)}/\text{TeV}^{-2} > 0$. The signal cross section driven by $\mathcal{O}_{uW}$ does not show such sensitivity to the sign of its Wilson coefficient, as it does not interfere with the SM.

(ii) $\mathcal{Z}$ decreases monotonically along bins of increasing p_{T12} for the operators, $\mathcal{O}_{Hq}^{(3)}$ and $\mathcal{O}_{Hq}^{(1)}$, while for $\mathcal{O}_{uW}$, $\mathcal{Z}$ steadily increases with p_{T12}. Significance, in each bin, is the joint outcome of how the SM and BSM contributions have their own p_{T12} dependence and what their interplay is. Any cross section in hadronic collision is a convolution of the partonic cross section with parton distribution functions (PDFs). PDFs decrease with increasing p_{T12} (higher collisional energy). The *signal* rate at the parton level either remains nearly independent of p_{T12} (for $\mathcal{O}_{Hq}^{(1)}$ and $\mathcal{O}_{Hq}^{(3)}$) or increases (for $\mathcal{O}_{uW}$) at a higher rate than the decrement of PDFs. Thus, in the latter case, enhancement of the EFT contribution with higher energy (p_{T12}) always improves the significance in high p_{T12} bins.

So far, we have presented the signal significance for a fixed integrated luminosity of 3000 fb^{-1}. However, we would also like to explore the luminosity required to obtain 3σ exclusion limits on $\frac{C_i}{\Lambda^2}$. To estimate the required luminosity, we have once again used the number of signal events in bins of p_{T12}, each of width 50 GeV, covering a range of 100–500 GeV for achieving 3σ significance as a function of the Wilson coefficient. This is shown for three operators in Fig. 8(a)–8(c). The vertical dotted dashed lines on each panel represent the intervals of $\frac{C_i}{\Lambda^2}$, which can be explored or ruled out at 3σ, with an integrated luminosity of 3000 fb^{-1}, marked by a horizontal line on each panel.

One can directly read from Fig. 8 the minimum luminosity required for signal with a given value of the Wilson coefficient, to be greater than 3σ fluctuation of background. Let us recall the 3σ limits on $\frac{C}{\Lambda^2}$ obtained by comparing the total cross section of the signal to background. $\frac{C_{Hq}^{(1)}}{\Lambda^2}$ has been constrained between -0.90 and 0.45 TeV^{-2} (see Fig. 7) with 3000 fb^{-1} of data. However, Fig. 8(a) tells us that a calculation of significance (with the same luminosity) in the p_{T12} bin of 100–150 GeV could impose a more severe limit of $(-0.29:0.21)$ TeV^{-2} on the same coupling. Similarly, the allowed region for $\frac{C_{Hq}^{(3)}}{\Lambda^2}$ becomes $(-0.09:0.15)$ TeV^{-2}, from the signal significance in the p_{T12} bin of 100–150 GeV. Finally, the allowed region for $\frac{C_{uW}}{\Lambda^2}$ becomes $(-0.12:0.12)$ TeV^{-2} calculated in the p_{T12} bin of 450–500 GeV. A comparison of the two above

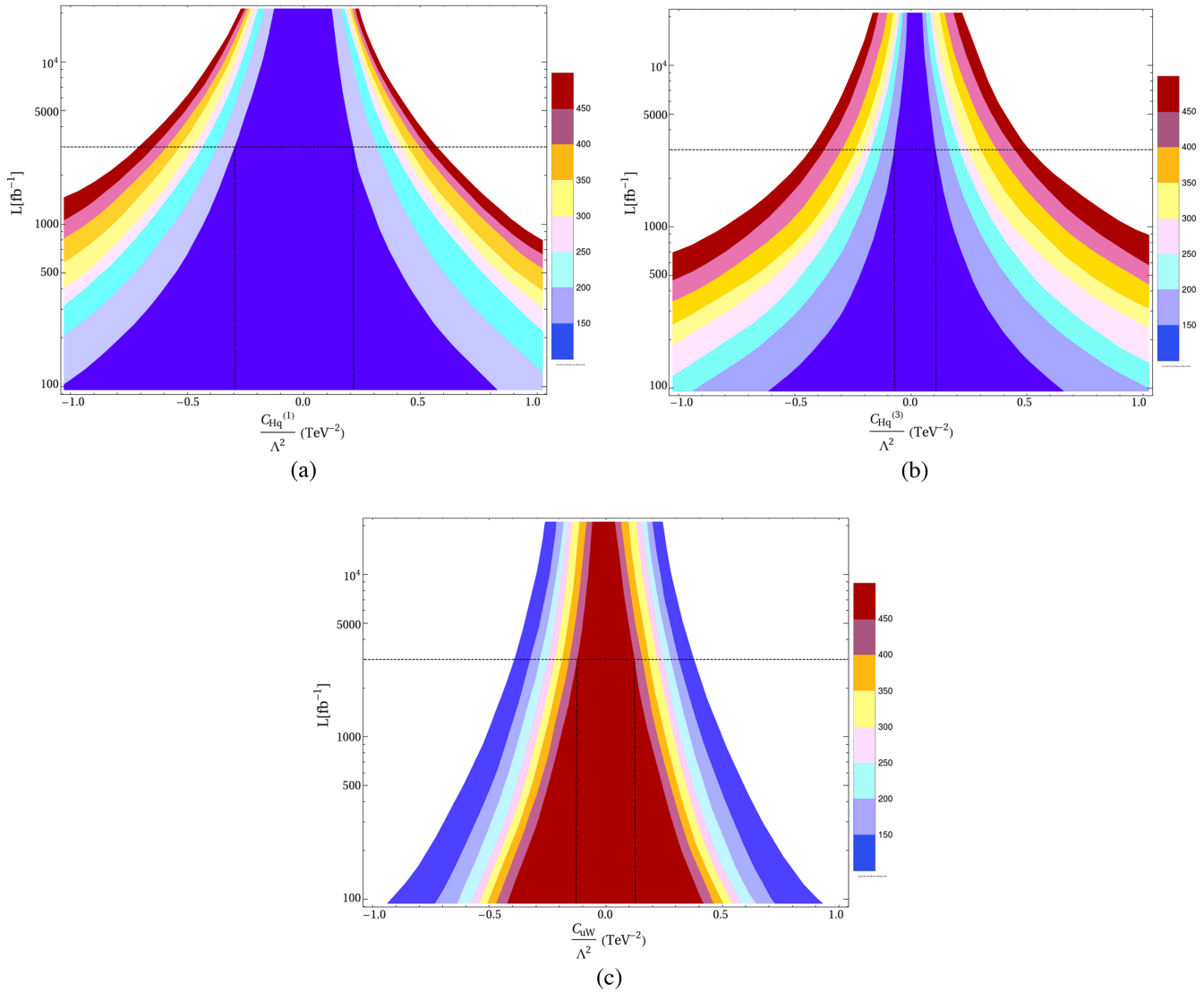

FIG. 8. Required integrated luminosity at 14 TeV for achieving a 3σ significance in bins of p_{T12} as a function of Wilson coefficients of operators (a)$\frac{C_{Hq}^{(1)}}{\Lambda^2}$, (b) $\frac{C_{Hq}^{(3)}}{\Lambda^2}$, and (c) $\frac{C_{uW}}{\Lambda^2}$. The different colored bands signify bins of p_{T12} each of width 50 GeV.

methods, thus, emphasizes the usefulness of sensitivity information in individual bins of p_{T12}. This guides us to the most profitable bins in looking for effects of SMEFT.

We have presented our results assuming one nonzero dimension-6 operator at a time. Before closing this section, let us discuss in brief the effect of two nonzero dimension-6 operators on the expected sensitivity to the signal. In Fig. 9, we have marked the regions in blue in the $\frac{C_{uW}}{\Lambda^2} - \frac{C_{Hq}^{(3)}}{\Lambda^2}$ plane, where a signal significance of 3 or more can be achieved. If no deviation is observed in the VBF Higgs production, we can obtain an upper limit on the Wilson coefficients at 2σ confidence level, which yields bounds on the Wilson coefficients at the 95% C.L. as shown in the yellow shaded region. A similar plot has been presented in the same figure with nonzero values of $\frac{C_{Hq}^{(1)}}{\Lambda^2}$ and $\frac{C_{Hq}^{(3)}}{\Lambda^2}$. For both the plots, any possible pair of values of the relevant couplings chosen from the blue region results in a signal away from 0 by at least 3 standard deviations. The correlation between the couplings shown in the plots can be understood by looking at the expression for the signal cross section in the case when C_{uW} and $C_{Hq}^{(3)}$ are taken nonzero at the same time:

$$\sigma(C_{uW}, C_{Hq}^{(3)}) = 0.653 + 0.27\left(\frac{C_{uW}}{\Lambda^2}\right)^2 + 0.167\left(\frac{C_{Hq}^{(3)}}{\Lambda^2}\right)^2 - 0.391\left(\frac{C_{Hq}^{(3)}}{\Lambda^2}\right). \quad (8)$$

For negative values of $C_{Hq}^{(3)}$, the interference term (linear in $C_{Hq}^{(3)}$) adds to the quadratic $(C_{Hq}^{(3)})^2$ term, and a relatively

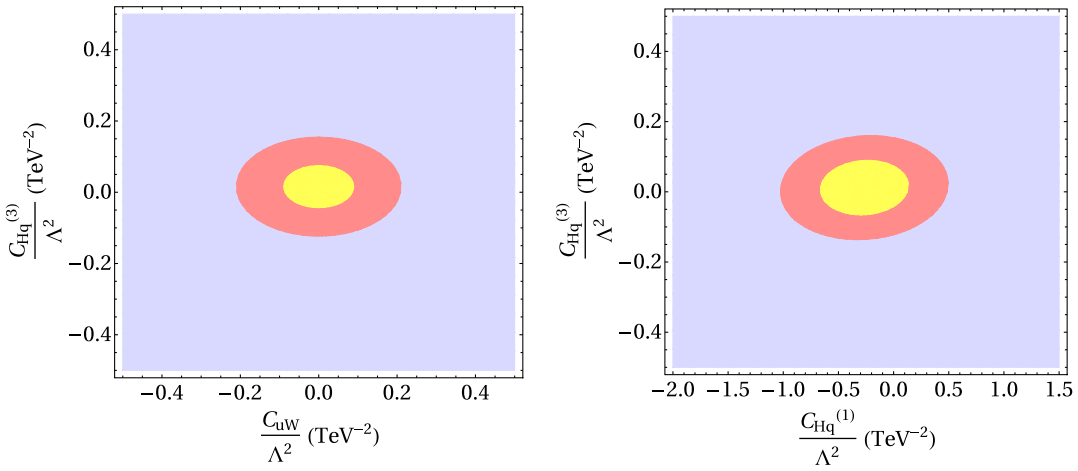

FIG. 9. Projections for a 3σ signal significance in blue shaded regions in the parameter space in (a) $\frac{C_{uW}}{\Lambda^2} - \frac{C_{Hq}^{(3)}}{\Lambda^2}$ and (b) $\frac{C_{Hq}^{(1)}}{\Lambda^2} - \frac{C_{Hq}^{(3)}}{\Lambda^2}$ planes with 3000 fb^{-1} data at 14 TeV run of the LHC. The 2σ level approximating the 95% confidence-level exclusion bounds are shown in yellow shaded regions.

smaller C_{uW} can achieve 3σ signal significance. On the other hand, for $C_{Hq}^{(3)}/\text{TeV}^2 > 0$, this destructive interference between the SM and $O_{Hq}^{(3)}$ will be compensated by both $(C_{uW})^2$ and $(C_{Hq}^{(3)})^2$ terms, meaning that the $\frac{1}{\Lambda^4}$ contribution helps to achieve a 3σ (or more) signal significance. The interval $|\frac{C_{uW}}{\Lambda^2}| > 0.22$ TeV^{-2} and $|\frac{C_{Hq}^{(3)}}{\Lambda^2}| > 0.15$ TeV^{-2} corresponds to a cross section of VBF Higgs production in the diphoton channel that is 7% away from the SM.

Similarly, in the $\frac{C_{Hq}^{(1)}}{\Lambda^2} - \frac{C_{Hq}^{(3)}}{\Lambda^2}$ plane, a correlation exists between the two. For $C_{Hq}^{(1)}/\text{TeV}^2 < 0$, the nature of its destructive interference with SM will be outweighed by the strong interference of $C_{Hq}^{(3)}$ in this range, and until $\frac{C_{Hq}^{(1)}}{\Lambda^2} < -1$ TeV^{-2}, its quadratic dependence takes over and adds to the total rate of the process. For $C_{Hq}^{(1)}/\text{TeV}^2 > 0$, although it interacts constructively with SM, the VBF process is more sensitive to $C_{Hq}^{(3)}$, and its destructive interference asks for a greater value of $c_{Hq}^{(1)}$. The above-mentioned pair of coefficients allows a region of parameter space which has, for instance, at $\frac{c_{Hq}^{(1)}}{\Lambda^2} = 0.4$ TeV^{-2}, $\frac{C_{Hq}^{(3)}}{\Lambda^2} = -0.2$ TeV^{-2}, a cross section 6% away from the SM value.

One can also check the effect of two operator couplings varying at the same time while estimating the signal significance in individual bins of p_{T12}. For instance, with 3000 fb^{-1} data, a 3σ difference can be achieved with $\frac{C_{uW}}{\Lambda^2} = \pm 0.23$ TeV^{-2} (while keeping the values of other couplings to zero) in the p_{T12} bin of 300–350 GeV [see Fig. 8(c)]. The effect of turning on $C_{Hq}^{(3)}$ along with C_{uW} can be easily understood from Eq. (8). With negative $C_{Hq}^{(3)}$, a 3σ effect can easily be achieved in the same bin with a smaller value of $\frac{C_{uW}}{\Lambda^2}$ than 0.23 TeV^{-2}.

All the results involving the dimension-6 operators, presented above, have been derived on the basis of LO estimation of cross section. To this end, we would like to comment on the possible inclusion of NLO QCD corrections to the new physics cross sections. We have estimated the NLO QCD corrected cross section for the VBF process involving the operators $\mathcal{O}_{Hq}^{(1)}$ and $\mathcal{O}_{Hq}^{(3)}$ which are available within the SMEFT@NLO [51] package. The following inferences can be drawn from our analysis. First, the total cross section at the NLO, as compared to LO, always goes up by the order 12%–25%. The k factors for the VBF process, calculated (from the total cross section) including $\mathcal{O}_{Hq}^{(1)}$ and $\mathcal{O}_{Hq}^{(3)}$ operators, are 1.12 and 1.25, respectively, assuming $\frac{C_i}{\Lambda^2} = 0.3$ TeV^{-2}. Furthermore, the overall orientation and shapes of the distributions (p_{T12}) are not significantly altered. Thus, our LO estimates are conservative in nature. We have also checked that uncertainty in the cross section due to factorization and renormalization scale choice at NLO is less than a percent when we change the scale from m_h to $\frac{m_h}{2}$. The differential k factors for both the operators are always greater than 1, becoming larger at high p_{T12} bins, reaching 1.25 and 1.29 in p_{T12} bins of 400–450 GeV, for $C_{Hq}^{(1)}$ and $C_{Hq}^{(3)}$, respectively. In cases in which the interference with the SM is constructive (depending on the sign of the Wilson coefficient of the operator), the bin-by-bin distinguishability with the pure SM contributions improves in most bins when NLO effects are included. In case of destructive interference, the distinguishability (from the SM) is adversely affected in the bins ranging from 150 to 350 GeV. However, there are always several bins where a significance above 3σ have been achieved with NLO cross section. In general,

high-p_T regions give better distinguishability on the inclusion of NLO effects.

V. SUMMARY AND CONCLUSION

We have considered the effects of some illustrative dimension-6 operators involving interaction of two quarks, Higgs field and a gauge boson and studied their potential effects on Higgs production via the vector boson fusion channel at the Large Hadron Collider. To begin with, we have obtained the upper limits on the Wilson coefficients of the aforementioned operators by a simple unitarity analysis of the process $qq \to hZ$, $qq \to hW$. The values of the Wilson coefficients used in our analysis are consistent with all the erstwhile experimental results including weak universality, electroweak precision tests, and LHC data. Parametrizing the strength of the new interactions by the coefficients $C_i(C_{Hq}^{(1)}, C_{Hq}^{(3)}, C_{uW})$, after a detailed cut-based Monte Carlo analysis, we study how the efficiencies of different acceptance cuts are altered for various values of C_i.

The final state considered in our study is a diphoton in association with two forward jets. We have utilized the jet kinematics to distinguish the signal from background. Our analysis does not depend on any particular decay mode of the Higgs boson. To be more specific, we find that the presence of these dimension-6 operators would result in harder p_T spectra of the two forward jets. Consequently, harder p_{T12} spectra will emerge on the inclusion of the effective operators discussed here. The present analysis has revealed a region in the $p_{T12} - \Delta\eta_{jj}$ phase space where the cases in the presence of dimension-6 operators along with the SM are populated with highly energetic jets and less separated in the rapidity direction. These regions define the new corners of phase space where the SM is highly depleted. Particularly, the operator with explicit momentum dependence affects the rapidity between the two leading jets and enhances their transverse momenta, most prominently. The other two operators that interfere with the SM also show similar effects to a lesser extent.

The VBF Higgs signal can be mimicked by processes like Higgs boson production with two jets via gluon fusion and non-Higgs background like dijet production with diphoton. With these backgrounds constituting nearly 80% of the true SM VBF cross section, we have computed the significance of our signal in two different ways: (i) by comparing the total cross section of signal and background and (ii) by comparing the signal and background event rates in the bins of p_{T12}. Significant improvement has been observed in obtaining 3σ limits on $\frac{C}{\Lambda^2}$ when significance calculation has been done in separate bins of p_{T12}. The projected 3σ upper limits for integrated luminosity of 3000 fb^{-1} from our analysis seem to be more restrictive than bounds coming from precision electroweak observables.

Several other kinematic observables can also be constructed out of the forward jets. We have specifically checked that in distributions of (i) the azimuthal angle difference of leading jet pairs, (ii) η centrality, and (iii) p_T difference of leading jet pair distribution sufficient modifications to SM predictions can be observed with moderate values of Wilson coefficients of these higher-dimensional operators. A study including these additional kinematic variables and their possible correlation, by going beyond the standard cut-based approach, will be reported in a follow-up study where other Higgs decay channels are also being taken into account.

ACKNOWLEDGMENTS

We thank Satyaki Bhattacharya for useful discussions. T. B. acknowledges the support from Council of Scientific and Industrial Research, Government of India. T. B. is thankful to Nabanita Ganguly and Tathagata Ghosh for insightful comments. The authors thank Satyanarayan Mukhopadhyay for a helpful discussion on the validity of EFT series.

[1] G. Aad *et al.* (ATLAS Collaboration), Observation of a new particle in the search for the Standard Model Higgs boson with the ATLAS detector at the LHC, Phys. Lett. B **716**, 1 (2012).
[2] S. Chatrchyan *et al.* (ATLAS Collaboration), Observation of a new boson at a mass of 125 GeV with the CMS experiment at the LHC, Phys. Lett. B **716**, 30 (2012).
[3] S. Weinberg, Phenomenological lagrangians, Physica A (Amsterdam) **96**, 327 (1979).
[4] W. Buchmüller and D. Wyler, Effective lagrangian analysis of new interactions and flavour conservation, Nucl. Phys. **B268**, 621 (1986).
[5] C. N. Leung, S. T. Love, and S. Rao, Low-energy manifestations of a new interaction scale: Operator analysis, Z. Phys. C **31**, 433 (1986).
[6] B. Henning, X. Lu, and H. Murayama, How to use the Standard Model effective field theory, J. High Energy Phys. 01 (2016) 023.
[7] S. Dawson, C. Englert, and T. Plehn, Higgs physics: It ain't over till it's over, Phys. Rep. **816**, 1 (2019).
[8] B. Grzadkowski, M. Iskrzynski, M. Misiak, and J. Rosiek, Dimension-six terms in the Standard Model Lagrangian, J. High Energy Phys. 10 (2010) 085.

[9] G. F. Giudice, C. Grojean, A. Pomarol, and R. Rattazzi, The strongly-interacting light Higgs, J. High Energy Phys. 06 (2007) 045.
[10] D. L. Rainwater, D. Zeppenfeld, and K. Hagiwara, Searching for $H \to \tau^+\tau^-$ in weak boson fusion at the CERN LHC, Phys. Rev. D **59**, 014037 (1998); V. Hankele, G. Klamke, D. Zeppenfeld, and T. Figy, Anomalous Higgs boson couplings in vector boson fusion at the CERN LHC, Phys. Rev. D **74**, 095001 (2006); T. Plehn, D. L. Rainwater, and D. Zeppenfeld, Determining the Structure of Higgs Couplings at the LHC, Phys. Rev. Lett. **88**, 051801 (2002); I. Low, J. Lykken, and G. Shaughnessy, Have we observed the Higgs (imposter)?, Phys. Rev. D **86**, 093012 (2012).
[11] C. Englert, A. Freitas, M. M. Mühlleitner, T. Plehn, M. Rauch, M. Spira, and K. Walz, Precision measurements of Higgs couplings: Implications for new physics scales, J. Phys. G **41**, 113001 (2014).
[12] S. Banerjee, S. Mukhopadhyay, and B. Mukhopadhyaya, Higher dimensional operators and the LHC Higgs data: The role of modified kinematics, Phys. Rev. D **89**, 053010 (2014).
[13] J. Ellis, V. Sanz, and T. You, Complete Higgs sector constraints on dimension-6 operators, J. High Energy Phys. 07 (2014) 036.
[14] A. Djouadi, R. M. Godbole, B. Mellado, and K. Mohan, Probing the spin-parity of the Higgs boson via jet kinematics in vector boson fusion, Phys. Lett. B **723**, 307 (2013).
[15] S. S. Biswal, R. M. Godbole, B. Mellado, and S. Raychaudhuri, Azimuthal Angle Probe of Anomalous HWW Couplings at a High Energy ep Collider, Phys. Rev. Lett. **109**, 261801 (2012).
[16] G. Amar, S. Banerjee, S. von Buddenbrock, A. S. Cornell, T. Mandal, B. Mellado, and B. Mukhopadhyaya, Exploration of the tensor structure of the Higgs boson coupling to weak bosons in e^+e^- collisions, J. High Energy Phys. 02 (2015) 128.
[17] V. Del Duca, W. Kilgore, C. Oleari, C. Schmidt, and D. Zeppenfeld, Gluon fusion contributions to $\mathrm{H}+2$ jet production, Nucl. Phys. **B616**, 367 (2001).
[18] D. de Florian *et al.* (LHC Higgs Cross Section Working Group), Handbook of LHC Higgs cross sections: 4. Deciphering the nature of the Higgs sector, arXiv:1610.07922.
[19] M. E. Peskin and T. Takeuchi, Estimation of oblique electroweak corrections, Phys. Rev. D **46**, 381 (1992).
[20] E. Massó and V. Sanz, Limits on anomalous couplings of the Higgs boson to electroweak gauge bosons from LEP and the LHC, Phys. Rev. D **87**, 033001 (2013).
[21] M. Farina, G. Panico, D. Pappadopulo, J. T. Ruderman, R. Torre, and A. Wulzer, Energy helps accuracy: Electroweak precision tests at hadron colliders, Phys. Lett. B **772**, 210 (2017).
[22] A. Falkowski, F. Riva, and A. Urbano, Higgs at last, J. High Energy Phys. 11 (2013) 111.
[23] M. B. Einhorn and J. Wudka, Higgs-boson couplings beyond the standard model, Nucl. Phys. **B877**, 792 (2013).
[24] J. Ellis, C. W. Murphy, V. Sanz, and T. You, Updated global SMEFT fit to Higgs, diboson and electroweak data, J. High Energy Phys. 06 (2018) 146.
[25] M. Cepeda, S. Gori, P. Ilten, M. Kado, F. Riva, R. A. Khalek, A. Aboubrahim, J. Alimena, S. Alioli and A. Alves *et al.*, Report from working group 2: Higgs physics at the HL-LHC and HE-LHC, CERN Yellow Rep. Monogr. **7**, 221 (2019).
[26] C. Englert, D. Goncalves-Netto, K. Mawatari, and T. Plehn, Higgs quantum numbers in weak boson fusion, J. High Energy Phys. 01 (2013) 148.
[27] I. Anderson, S. Bolognesi, F. Caola, Y. Gao, A. V. Gritsan, C. B. Martin, K. Melnikov, M. Schulze, N. V. Tran, A. Whitbeck *et al.*, Constraining anomalous HVV interactions at proton and lepton colliders, Phys. Rev. D **89**, 035007 (2014).
[28] C. Degrande, B. Fuks, K. Mawatari, K. Mimasu, and V. Sanz, Electroweak Higgs boson production in the standard model effective field theory beyond leading order in QCD, Eur. Phys. J. C **77**, 262 (2017).
[29] T. G. Rizzo, Searching for anomalous weak couplings of heavy flavors at the SLC and LEP, Phys. Rev. D **51**, 3811 (1995).
[30] S. Schael *et al.* (ALEPH, DELPHI, L3, OPAL, SLD, LEP Electroweak Working Group, SLD Electroweak Group and SLD Heavy Flavour Group), Precision electroweak measurements on the Z resonance, Phys. Rep. **427**, 257 (2006).
[31] G. F. Giudice, P. Paradisi, and M. Passera, Testing new physics with the electron g-2, J. High Energy Phys. 11 (2012) 113.
[32] P. A. Zyla *et al.* (Particle Data Group), Review of particle physics, Prog. Theor. Exp. Phys. **2020**, 083C01 (2020).
[33] M. Aaboud *et al.* (ATLAS Collaboration), Observation of $H \to b\bar{b}$ decays and VH production with the ATLAS detector, Phys. Lett. B **786**, 59 (2018).
[34] A. M. Sirunyan *et al.* (CMS Collaboration), Observation of Higgs Boson Decay to Bottom Quarks, Phys. Rev. Lett. **121**, 121801 (2018).
[35] M. Aaboud *et al.* (ATLAS Collaboration), Cross-section measurements of the Higgs boson decaying into a pair of τ-leptons in proton-proton collisions at $\sqrt{s} = 13$ TeV with the ATLAS detector, Phys. Rev. D **99**, 072001 (2019).
[36] A. M. Sirunyan *et al.* (CMS Collaboration), Observation of the Higgs boson decay to a pair of τ leptons with the CMS detector, Phys. Lett. B **779**, 283 (2018).
[37] A. Alloul, N. D. Christensen, C. Degrande, C. Duhr, and B. Fuks, FeynRules 2.0—A complete toolbox for tree-level phenomenology, Comput. Phys. Commun. **185**, 2250 (2014).
[38] J. Alwall, R. Frederix, S. Frixione, V. Hirschi, F. Maltoni, O. Mattelaer, H.-S. Shao, T. Stelzer, P. Torrielli, and M. Zaro, The automated computation of tree-level and next-to-leading order differential cross sections, and their matching to parton shower simulations, J. High Energy Phys. 07 (2014) 079.
[39] R. D. Ball *et al.*, Parton distributions with LHC data, Nucl. Phys. **B867**, 244 (2013).
[40] T. Sjostrand, S. Mrenna, and P. Z. Skands, PYTHIA 6.4 physics and manual, J. High Energy Phys. 05 (2006) 026.
[41] J. Favereau, C. Delaere, P. Demin, A. Giammanco, V. Lemaître, A. Mertens, and M. Selvaggi (DELPHES 3 Collaboration), DELPHES 3, A modular framework for fast simulation of a generic collider experiment, J. High Energy Phys. 02 (2014) 057.

[42] M. Cacciari, G. P. Salam, and G. Soyez, FASTJET user manual, Eur. Phys. J. C **72**, 1896 (2012).
[43] M. Aaboud *et al.* (ATLAS Collaboration), Measurements of Higgs boson properties in the di-photon decay channel with 36 fb^{-1} of pp collision data at $\sqrt{s} = 13$ TeV with the ATLAS detector, Phys. Rev. D **98**, 052005 (2018).
[44] J. Y. Araz, S. Banerjee, R. S. Gupta, and M. Spannowsky, Precision SMEFT bounds from the VBF Higgs at high transverse momentum, J. High Energy Phys. 04 (2021) 125.
[45] P. Nason and C. Oleari, NLO Higgs boson production via vector-boson fusion matched with shower in POWHEG, J. High Energy Phys. 02 (2010) 037; F. Maltoni, K. Mawatari, and M. Zaro, Higgs characterisation via vector-boson fusion and associated production: NLO and parton-shower effects, Eur. Phys. J. C **74**, 2710 (2014); M. Cacciari, F. A. Dreyer, A. Karlberg, G. P. Salam, and G. Zanderighi, Fully Differential Vector-Boson-Fusion Higgs Production at Next-to-Next-to-Leading Order, Phys. Rev. Lett. **115**, 082002 (2015); Erratum, Phys. Rev. Lett. **120**, 139901 (2018).
[46] P. Bolzoni, F. Maltoni, S. O. Moch, and M. Zaro, Higgs Production Via Vector-Boson Fusion at NNLO in QCD, Phys. Rev. Lett. **105**, 011801 (2010).
[47] R. Contino, A. Falkowski, F. Goertz, C. Grojean, and F. Riva, On the validity of the effective field theory approach to SM precision tests J. High Energy Phys. 07 (2016) 144.
[48] J. Baglio, S. Dawson, S. Homiller, S. D. Lane, and I. M. Lewis, Validity of standard model EFT studies of VH and VV production at NLO, Phys. Rev. D **101**, 115004 (2020).
[49] G. Cowan, K. Cranmer, E. Gross, and O. Vitells, Asymptotic formulae for likelihood-based tests of new physics, Eur. Phys. J. C **71**, 1554 (2011).
[50] ATLAS Collaboration, Projections for measurements of Higgs boson cross sections, branching ratios and coupling parameters with the ATLAS detector at a HL-LHC, No. ATL-PHYS-PUB-2013-014.
[51] C. Degrande, G. Durieux, F. Maltoni, K. Mimasu, E. Vryonidou, and C. Zhang, Automated one-loop computations in the standard model effective field theory, Phys. Rev. D **103**, 096024 (2021).